

# Electroexcitation of nucleon resonances at $Q^2 = 0.65 \text{ (GeV/c)}^2$ from a combined analysis of single- and double-pion electroproduction data

I.G. Aznauryan,<sup>1,2</sup> V.D. Burkert,<sup>1</sup> G.V. Fedotov,<sup>3</sup> B.S. Ishkhanov,<sup>3</sup> and V.I. Mokeev<sup>1,3</sup>

<sup>1</sup> Thomas Jefferson National Accelerator Facility, Newport News, Virginia 23606, USA

<sup>2</sup> Yerevan Physics Institute, 375036 Yerevan, Armenia

<sup>3</sup> Skobeltsyn Nuclear Physics Institute at Moscow State University, 119899 Moscow, Vorobey gory, Russia

Data on single- and double-charged pion electroproduction off protons are successfully described in the second and third nucleon resonance regions with common  $N^*$  photocouplings. The analysis was carried out using separate isobar models for both reactions. From the combined analysis of two exclusive channels, the  $\gamma^*p \rightarrow N^{*+}$  helicity amplitudes are obtained for the resonances  $P_{11}(1440)$ ,  $D_{13}(1520)$ ,  $S_{31}(1620)$ ,  $S_{11}(1650)$ ,  $F_{15}(1680)$ ,  $D_{33}(1700)$ ,  $D_{13}(1700)$ , and  $P_{13}(1720)$  at  $Q^2 = 0.65 \text{ (GeV/c)}^2$ .

PACS numbers: PACS number(s): 13.40.Gp, 13.60.Le, 14.20.Gk

## I. INTRODUCTION

Our knowledge of electromagnetic excitations of nucleon resonances is mostly given by single-pion photo- and electroproduction experiments [1]. The only exception is the  $S_{11}(1535)$  resonance, which is strongly revealed in photo- and electroproduction of  $\eta$  and is well investigated in these processes (see, for example, Refs. [2, 3, 4, 5, 6, 7, 8, 9]). Although with increasing masses, the couplings of the resonances to multi-pion channels become increasingly significant, and for many resonances dominant, the scarcity of experimental data made it impossible to investigate properties of nucleon resonances in the photo- and electroproduction reactions with final states different from  $\pi N$  and  $\eta N$ .

The situation changed recently, when precise measurements of single- and double-pion electroproduction were carried out at Jefferson Lab with the CEBAF Large Acceptance Spectrometer (CLAS). In double-charged pion electroproduction on protons, the  $\pi^+p$ ,  $\pi^-p$ ,  $\pi^+\pi^-$  invariant mass distributions, c.m.s.  $\pi^-$  angular distributions, and total cross sections were obtained in the second, third, and partly fourth resonance regions at  $Q^2$  from 0.5 to 1.5  $(\text{GeV/c})^2$  [10, 11]. At these  $Q^2$ , the CLAS measurements of single pion electroproduction on protons include differential cross sections and polarized beam asymmetries for  $\pi^0$  and  $\pi^+$  electroproduction [11, 12, 13, 14, 15]. Complemented with older DESY and NINA data [16, 17, 18, 19, 20],  $\pi^0$  and  $\pi^+$  cross sections extend from threshold to the third resonance region. Polarized beam asymmetry measurements cover first and second resonance regions.

Using these measurements, we have carried out a combined analysis of single- and double-pion electroproduction data at  $Q^2 = 0.65 \text{ (GeV/c)}^2$  in the second and third resonance regions. For this kinematics, the most complete set of data for the two channels is available. In this paper, we report on the results of this analysis, which was carried out using independent isobar models for each channel, but with common  $N^*$  photocouplings.

Reliable description of non-resonant mechanisms, as

well as separation of resonant and background contributions represent fundamental problems in  $N^*$  studies. Presently, non-resonant processes can be treated only at a phenomenological level. Reliability of background description and resonance/background separation can be put to the test in combined analyses of major exclusive channels. Single- and double-pion channels in meson photo- and electroproduction account for almost 90% of the total cross section in the  $N^*$  excitation region. In addition, these production channels have completely different backgrounds. A successful description of these channels combined would confirm the reliability of the background description and resonance/background separation. Therefore, this way we expect to obtain the most accurate values for  $N^*$  photocouplings with considerably reduced model uncertainties arising from the phenomenological separation of resonances and background.

The analysis of two exclusive channels of pion electroproduction on protons has been performed within isobar models which are presented in Section 2. The analysis and the results are presented in Section 3. In this section, we will demonstrate that the two main exclusive channels can be described with the same values of  $N^*$  photocouplings for the resonances from the second and third resonance regions. The sets of the  $\gamma^*p \rightarrow N^{*+}$  helicity amplitudes will be found that give minimal  $\chi^2$  values, fitting single- and double-pion electroproduction data simultaneously. The conclusions are presented in Section 4.

## II. THE ANALYSIS TOOLS

### A. Single pion electroproduction

The analysis of single pion electroproduction data has been performed within the isobar model presented in Refs. [8, 21]. In Ref. [21], this model was successfully used to describe multipole amplitudes of the GWU(VPI) [22, 23] partial-wave analysis of  $\pi$  photoproduction data. It was also successfully used for the anal-

ysis of CLAS data on  $\pi$  electroproduction at  $Q^2 = 0.4$  and  $0.65 \text{ (GeV/c)}^2$  [8]. The model consists of resonance contributions parametrized in the Breit-Wigner form and non-resonance background built from the Born term (the  $s$  and  $u$  channel nucleon exchanges and  $t$  channel  $\pi$  contribution) and the  $t$  channel  $\rho$  and  $\omega$  contributions. The background is unitarized in the  $K$ -matrix approximation. With increasing energy, the background transforms into the amplitudes in the Regge pole regime. In the present analysis the background was fixed in the way described in Ref. [8], where at  $Q^2 = 0.65 \text{ (GeV/c)}^2$  the analysis of the same data was done, focusing on the  $N^*$  mass region below  $1.54 \text{ GeV}$ .

### B. Double-pion electroproduction

The analysis of two-pion electroproduction data was performed within the JLAB-MSU (Jefferson Lab - Moscow State University) isobar model [24]. It incorporates significant improvements over the approach of Refs. [25, 26], which was used in the analysis of CLAS  $2\pi$  electroproduction data in Ref. [10].

In the initial version of the isobar model [25, 26], double-charged-pion production was described by superposition of the following quasi-two-body channels with formation and subsequent decay of unstable particles in the intermediate states:

$$\gamma p \rightarrow \pi^- \Delta^{++} \rightarrow \pi^- \pi^+ p, \quad (1)$$

$$\gamma p \rightarrow \pi^+ \Delta^0 \rightarrow \pi^+ \pi^- p, \quad (2)$$

$$\gamma p \rightarrow \rho^0 p \rightarrow \pi^+ \pi^- p. \quad (3)$$

Remaining (residual) mechanisms were parametrized as 3-body phase space with the amplitude fitted to the data. This amplitude was a function of photon virtuality  $Q^2$  and the invariant mass of final hadronic system  $W$  only. In this approach, we were able to reproduce the main features of integrated cross sections, as well as invariant masses  $M_{\pi^+\pi^-}$ ,  $M_{\pi^+p}$  of  $\pi^+\pi^-$ ,  $\pi^+p$  systems, and  $\pi^-$  angular distributions.

The data on  $\pi^-p$  invariant mass distributions revealed evidence for the new isobar channel [24]:

$$\gamma p \rightarrow \pi^+ D_{13}^0(1520) \rightarrow \pi^+ \pi^- p. \quad (4)$$

This mechanism allows us to describe an excess of strength measured in the  $\pi^-p$  invariant mass distributions with respect to those calculated in the initial version of the JLAB-MSU model. This extra strength in the data, located around  $1.52 \text{ GeV}$  in  $\pi^-p$  invariant mass distributions, was clearly seen for all measured  $W$  bins kinematically allowed for the reaction (4). The production amplitudes for the first three quasi-two-body mechanisms (1-3) were treated as sums of  $N^*$  excitations in the  $s$ -channel and non-resonant mechanisms described in Refs. [25, 26]. The quasi-two-body mechanism (4) was entirely treated as a non-resonant process [24]. In reactions (1-3), all well established 4-star resonances with observed decays to the two-pion final states were included as

well as the 3-star states  $D_{13}(1700)$ ,  $P_{11}(1710)$ ,  $P_{33}(1600)$ . For the latter state a  $1.67 \text{ GeV}$  mass was obtained in our fit. This value is in agreement with the results of recent analyses of the  $\pi N$  scattering experiments [27]. The electromagnetic couplings for the  $\gamma p \rightarrow N^{*+}$  vertices were fitted to the data. Hadronic coupling constants for  $N^* \rightarrow \pi \Delta$  and  $\rho p$  decays were taken from the analyses of experiments with hadronic probes in the way described in Ref. [25]. The hadronic parameters for a possible new baryon state  $3/2^+(1720)$ , which has manifested itself in the CLAS  $2\pi$  photo- and electroproduction data [10, 28], were determined from a fit to the electroproduction data. The hadronic couplings for  $P_{13}(1720)$ ,  $D_{13}(1700)$ ,  $P_{33}(1600)$  were also found from fits to the CLAS  $2\pi$  electroproduction data.

In the improved JLAB-MSU model, we have also modified the contribution from residual mechanisms. While the initial version of the model succeeded in reproducing  $\pi^+\pi^-$ ,  $\pi^+p$  mass distributions, it had shortcomings in the description of the c.m.  $\pi^-$  angular distributions at low  $W$  (dashed lines in Fig. 1). The 3-body phase space description of residual mechanisms was replaced by the set of exchange terms shown in Fig. 2. This allowed a better description of the  $\pi^-$  angular distributions (solid lines in Fig. 1) in the entire  $Q^2$  range covered by CLAS measurements.

The amplitudes of mechanisms shown in Fig. 2 were parametrized in the Lorentz invariant form as follows:

$$A(W, Q^2) [\varepsilon_\mu^\gamma \bar{U}_{p'} \gamma^\mu U_p] (P_1 P_2) e^{b(P_\mu^2 - P_{\mu, \min}^2)}, \quad (5)$$

where  $\varepsilon_\mu^\gamma$  is the photon vector,  $U_p, \bar{U}_{p'}$  are the spinors for the initial and final protons,  $P_\mu^2$  is the square of the 4-momentum transfer in the exchange process, and  $P_{\mu, \min}^2$  is the minimal allowed value of this quantity. In Eq. (5), we have introduced the scalar product of four momenta  $(P_1 P_2)$  for the pairs of particles produced in the diagram vertices; this allowed us to reproduce the shapes of the corresponding invariant mass distributions. Following the diffractive ansatz, successfully used for the description of vector meson photo- and electroproduction, we have parametrized the propagators in the exchange diagrams shown in Fig. 2 as exponential functions of  $P_\mu^2 - P_{\mu, \min}^2$ . Parameter  $b$  is the constant value found from the fit to the data. The overall strength for each exchange mechanism was adjusted to the data. We required smooth, structureless behavior of cross-sections from these mechanisms as a function of  $W$ . The sub-processes with  $\pi^-$  in lower vertices of the Fig. 2 diagrams create backward peaks in the  $\pi^-$  angular distributions. These are mechanisms which allowed us to reproduce angular distributions at backward angles in the entire kinematics region covered by the CLAS measurements. The sub-processes with  $\pi^-$  in the upper vertices were necessary to provide good description of mass distributions, as well as of the  $\pi^-$  angular distributions at forward angles at  $W \geq 1.7 \text{ GeV}$ .

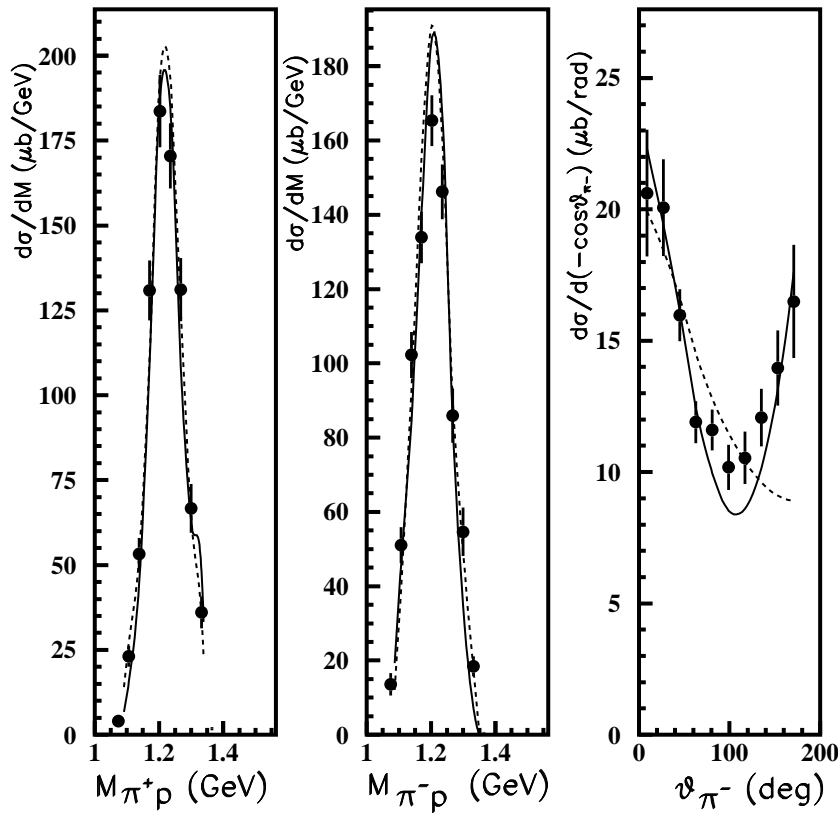


FIG. 1: CLAS  $2\pi$  electroproduction data [10] in comparison with the results of the fits within the initial (dashed lines) and improved (solid lines) JLAB-MSU model.  $W=1.49$  GeV,  $Q^2=0.65$  ( $\text{GeV}/c$ ) $^2$ .

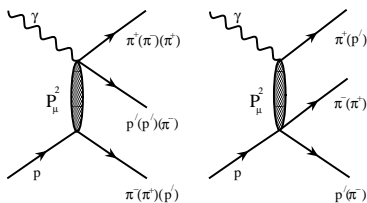


FIG. 2: Exchange background mechanisms for  $2\pi$  production, implemented in improved JLAB-MSU model.

With the improved JLAB-MSU model, a much better description of the data was obtained.

### III. THE ANALYSIS AND RESULTS

The database for single-pion electroproduction includes both recent CLAS and older NINA and DESY data on protons, in particular:

(a) the CLAS data on  $\pi^0$  cross sections ( $W = 1.1 - 1.52$  GeV,  $E_e = 1.645$  GeV and  $W = 1.1 - 1.68$  GeV,

$E_e = 2.445$  GeV) [12],  $\pi^+$  cross sections ( $W = 1.1 - 1.41$  GeV) [13], and polarized beam asymmetry in  $\pi^0$  and  $\pi^+$  electroproduction ( $W = 1.1 - 1.58$  GeV) [14, 15];

(b) the DESY and NINA data on  $\pi^0$  and  $\pi^+$  differential cross sections at  $W = 1.4 - 1.78$  GeV [16, 17, 18, 19, 20].

Therefore, the data used in the analysis of single-pion electroproduction include first, second, and third resonance regions. The data in the third resonance region consist of CLAS data on  $\pi^0$  differential cross sections, and the DESY and NINA data which, unlike CLAS measurements with full angular coverage, extend mostly over limited ranges of angles. 9870 data points were analyzed in the one-pion channel.

The two-pion electroproduction data are all from CLAS. They cover the  $W$ -range from 1.4 to 1.9 GeV, and are composed of 20  $W$ -bins with 0.025 GeV bin width. Each bin contains data on  $\pi^+\pi^-$ ,  $\pi^+p$ ,  $\pi^-p$  invariant mass (8 points for each cross-section) and  $\pi^-$  angular distributions (10 points). Overall 680 data points were fitted.

In the analysis we have taken into account all 4 and 3 star resonances from the second and third resonance regions. The parameters of these resonances are listed in

Table 1. Along with the ranges taken from RPP [29], we have presented the values of masses and widths used in the fits; these values were fixed. We have also presented the values of branching ratios used for extraction of helicity amplitudes for the  $\gamma^*N \rightarrow N^*$  transitions. At  $Q^2 = 0$ , the couplings of the resonances  $P_{33}(1600)$ ,  $D_{15}(1675)$  and  $P_{11}(1710)$  to  $\gamma N$  are small. Our analysis showed that these resonances have minor contributions to the resonant electroproduction cross sections. By this reason, the states  $P_{33}(1600)$ ,  $D_{15}(1675)$  and  $P_{11}(1710)$  are not listed in Table 1. The photocouplings of the  $P_{11}(1710)$  were taken equal to 0, since any significant contribution from this state spoiled the shapes of  $\pi^+\pi^-$  mass distributions in  $2\pi$  electroproduction data. The absolute values of the helicity amplitudes for the  $\gamma^*p \rightarrow P_{33}^+(1600)$  and  $\gamma^*N \rightarrow D_{15}^+(1675)$  transitions obtained in our analysis were below  $0.02 \text{ GeV}^{-1/2}$ . The  $S_{11}(1535)$  resonance has small branching ratio to the  $\pi\pi N$  channel; it was included only in the analysis of single-pion electroproduction data. In that analysis, we have also included the  $P_{33}(1232)$  resonance; its parameters were fixed according to the results obtained in Ref. [8].

The combined analysis of  $\pi$  and  $2\pi$  electroproduction data was made in several steps which are presented below.

### A. Step 1

We started with the description of single-pion electroproduction data. The observables mentioned above were evaluated within the framework of the unitary isobar model [8, 21]. The helicity amplitudes for the  $\gamma^*p \rightarrow N^{*+}$  transitions were the only free parameters fitted to the data. The parameters of the model related to the background (Born term and  $\rho$  and  $\omega$  contributions) were fixed according to Ref. [8]. Masses, widths and  $\pi N$  branching ratios of the resonances were fixed at the values given in Table 1. Values of photocouplings and their uncertainties were obtained via minimization of  $\chi^2$  over all data points using the MINUIT package [30]. The obtained results are presented in Table 2 in the columns corresponding to "1 $\pi$  analysis". The value of  $\chi^2/(\text{data points})$  over all data was 1.19. The quoted errors are the fit uncertainties corresponding to the global  $\chi^2$  minimum.

The results for the resonances  $P_{11}(1440)$ ,  $D_{13}(1520)$  listed in Table 2, and for the  $S_{11}(1535)$ , coincide with those obtained in Ref. [8], where at  $Q^2 = 0.65 \text{ (GeV/c)}^2$  the analysis of the same data was done.

### B. Step 2

Further, taking into account the results of the "1 $\pi$  analysis", the  $2\pi$  electroproduction data [10] were analyzed within the framework of the improved JLAB-MSU model. The transverse electroexcitation helicity amplitudes  ${}_pA_{1/2}$ ,  ${}_pA_{3/2}$  for the resonances with  $M <$

$1.7 \text{ GeV}$  were varied around the values, obtained in step 1, because these resonances have large branching ratios to the  $\pi N$  channel, and therefore, their amplitudes found in step 1 are good starting values for the  $2\pi$  electroproduction data fit. The only exception is the amplitude  ${}_pA_{1/2}$  for the  $P_{11}(1440)$ , as its values found in Ref. [8] using different approaches (isobar model and dispersion relations) were significantly different. In our analysis of  $2\pi$  electroproduction data, this amplitude was varied inside the range which overlapped the values reported in Ref. [8]. For the resonances with  $M \geq 1.7 \text{ GeV}$ , which decay mostly to the  $\pi\pi N$  channel, initial values of transverse amplitudes were taken from the previous analysis [31] of  $2\pi$  electroproduction data within initial version of the JLAB-MSU model. The initial values of all longitudinal amplitudes  ${}_pS_{1/2}$  were taken from step 1. As the values of  ${}_pS_{1/2}$  for the resonances  $D_{13}(1700)$  and  $P_{13}(1720)$  found in step 1 were compatible with 0, they were taken equal to zero and kept unchanged in the fitting procedure.

Among the resonances listened in Table 1, there are two strongly excited states in single-pion electroproduction which play an important role in the description of the data:  $D_{13}(1520)$  and  $F_{15}(1685)$ . The resonance  $D_{13}(1520)$  contributes almost half of the resonant cross sections in the second resonance region and is responsible for correct description of angular dependencies of the cross sections and polarized beam asymmetries in this region.  $F_{15}(1685)$  gives large contribution to the resonant  $\pi$  electroproduction cross section in the third resonance region; its contribution is very important for the description of angular dependencies in this region. These resonances were also observed in  $\pi\pi N$  channel with considerable excitation strengths [31]. To study the sensitivity of photocouplings for the  $D_{13}(1520)$  and  $F_{15}(1685)$  to single- and double-pion production data, we performed two separate fits of the  $2\pi$  electroproduction data with different ranges of sampling for  $N^*$  photocouplings.

Initial values of helicity amplitudes were sampled according to normal distribution. The variations  $\sigma$  were taken equal to 30% for all states, except  $D_{13}(1520)$ ,  $F_{15}(1685)$ , and the  ${}_pA_{1/2}$  amplitude for the  $P_{11}(1440)$ , which was varied inside the range obtained in Ref. [8]. In the first fit (Fit A), the photocouplings of  $D_{13}(1520)$  and  $F_{15}(1685)$  were varied inside uncertainties obtained at step 1. So in this fit, we assumed that the  $D_{13}(1520)$ ,  $F_{15}(1685)$  photocouplings were driven by single-pion electroproduction. The second fit (Fit B) was performed by varying these photocouplings with  $\sigma$  equal to 30 %. The amplitudes of the exchange diagrams shown in Fig. 2 were varied in both fits within 20%, applying W-independent multiplicative factors for each mechanism. The range of calculated differential cross sections overlapped entirely the measured cross sections, showing that actual values of  $N^*$  photocouplings are inside intervals adopted for the photocoupling variations. For each set of  $N^*$  photocouplings, the value of  $\chi^2$  was estimated. Further, we have selected the sets of  $N^*$  photocouplings, corresponding to values of  $\chi^2$ , when deviation between

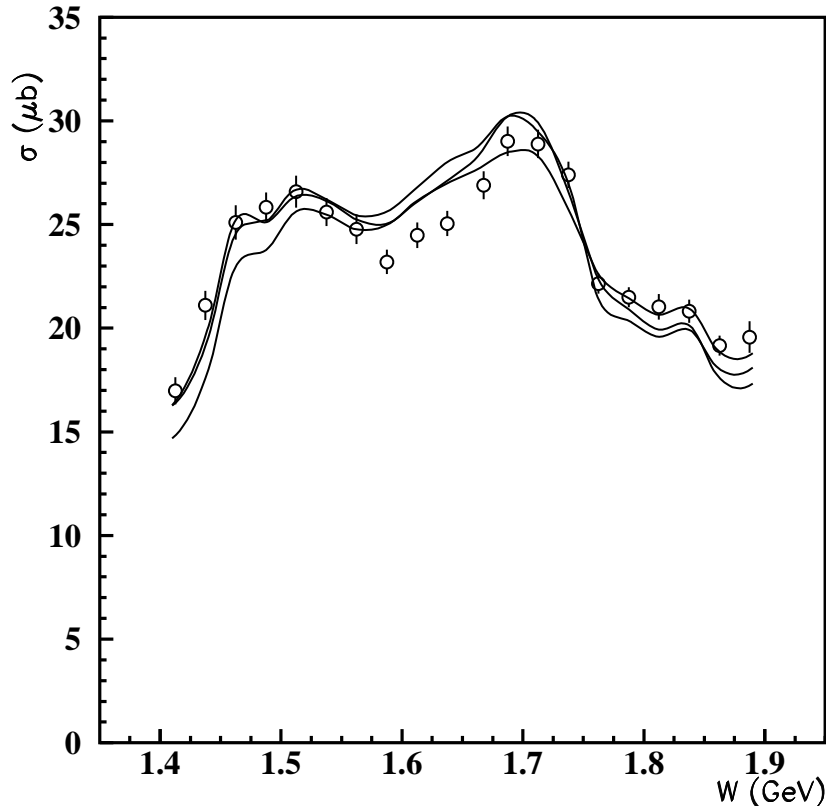


FIG. 3: Description of CLAS data [10] on total double charged pion electroproduction cross sections with  $N^*$  photocouplings taken from step 1. Solid lines corresponds to the closest to the data calculated cross sections.

calculated cross sections and the data were inside the uncertainties of the measurements. This minimization procedure for Fit A finally left us with 16 sets of  $N^*$  photocouplings with  $2.81 < \chi^2/(\text{data point}) < 3$ . All these photocouplings allowed us to get good description of  $2\pi$  electroproduction data. A similar minimization procedure for Fit B gave us additional 6 sets of  $N^*$  photocouplings with  $2.83 < \chi^2/(\text{data point}) < 2.95$ . So Fit B did not allow us to improve the description for the  $2\pi$  electroproduction data set with respect to Fit A, where  $D_{13}(1520)$  and  $F_{15}(1685)$  photocouplings were driven by the data on single-pion electroproduction.

The sets of  $N^*$  photocouplings selected in Fit A and Fit B were averaged. Mean values were assigned to the extracted  $N^*$  photocouplings, while dispersions were treated as the photocoupling uncertainties. The obtained amplitudes are presented in Table 2 as " $2\pi$  analysis (step 2)" results. The ranges of photocouplings were evaluated not from the global minimum for  $\chi^2$ , but by applying restriction  $\chi^2/(\text{data point}) < 3$ . In this way we have achieved more realistic accounting of the influence of data uncertainties on the extracted  $N^*$  photocouplings. We also took into account the possibility of having multiple

compatible descriptions of the data with close  $\chi^2$ .

As seen from Table 2, for the resonances with considerable decay rates to the  $\pi N$  final state ( $P_{11}(1440)$ ,  $D_{13}(1520)$ ,  $S_{11}(1650)$ ,  $F_{15}(1680)$ ), as well as for  $D_{33}(1700)$ , which decays mostly to  $\pi\pi N$ , the photocouplings extracted in the analyses of single- and double-pion electroproduction data are compatible within errors and the uncertainty of the  $P_{11}(1440)$   $pA_{1/2}$  amplitude extraction from  $\pi$  electroproduction.

For the resonances  $S_{31}(1620)$ ,  $D_{13}(1700)$ , and  $P_{13}(1720)$  with considerable decay rates to the  $\pi\pi N$  final state, the photocouplings extracted in analyses of single- and double-pion electroproduction data are different. To understand the importance of this difference for the description of  $2\pi$  electroproduction data, we tried to fit these data using  $N^*$  photocouplings sampled within the ranges determined from single-pion data analysis. We selected 3 solutions with smallest  $\chi^2$ :  $\chi^2/(\text{data point}) = 3.4$ -3.9. These values of  $\chi^2$  are significantly larger than those obtained in unconstrained analysis of  $2\pi$  electroproduction data. The  $2\pi$  electroproduction total cross sections corresponding to 3 selected solutions are shown in comparison with the data in Fig. 3. It

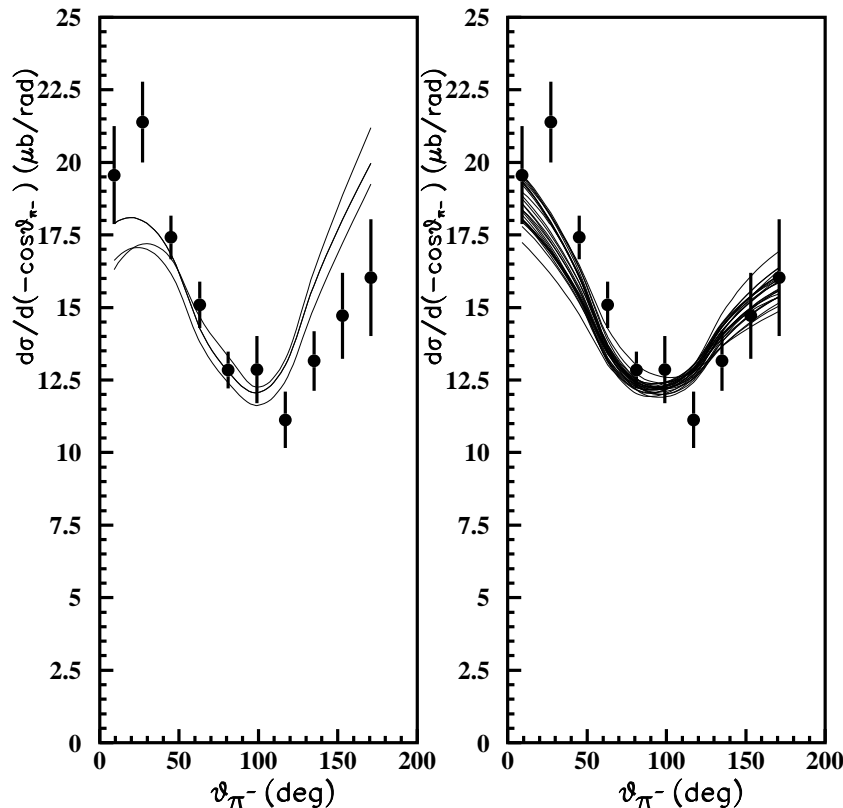


FIG. 4: Description of CLAS  $2\pi$  electroproduction data [10] on  $\pi^-$  angular distributions at  $W=1.71$  GeV,  $Q^2=0.65$   $(GeV/c)^2$ . Left: closest to the data cross sections calculated with  $N^*$  photocouplings obtained in " $1\pi$  analysis". Right: cross sections with  $N^*$  photocouplings found in " $2\pi$  analysis".

can be seen that there is an excess in the calculated cross sections at  $W$  between 1.56 and 1.7 GeV, which suggests that the values of the  $S_{31}(1620)$  photocouplings derived from single-pion electroproduction are overestimated. The reduction of the photoexcitation strength for this state to the value derived from the fit in the  $\pi\pi N$  channel is vital to reproduce double pion electroproduction data at  $W = 1.56 - 1.7$  GeV. As for the  $D_{13}(1700)$  and  $P_{13}(1720)$  photocouplings, if we would restrict their values by the ranges obtained in  $\pi$  electroproduction data analysis, we would fail to reproduce  $\pi^-$  angular distributions in the backward hemisphere as is shown in Fig. 4. On the left part of this plot we compare the data with the cross sections calculated using 3 sets of  $N^*$  photocouplings taken from the results of the single-pion data analysis. Unrestricted fit of  $2\pi$  electroproduction data allows us to reproduce very well the angular distributions at  $W$  around 1.7 GeV, as is shown in the right part of Fig. 4.

### C. Step 3

At this stage of the analysis we have finally found the ranges of the  $\gamma^*p \rightarrow N^{*+}$  helicity amplitudes which allow us to obtain a good description of electroproduction data in both  $\pi N$  and  $\pi\pi N$  channels. First, for each of 16 sets of  $N^*$  photocouplings found at Fit A of the previous step, we have estimated the value of  $\chi^2$  for single-pion electroproduction from comparison between measured and calculated observables. It turned out that there are 3 sets of helicity amplitudes that give the smallest values of  $\chi^2$  simultaneously in single- and double-pion electroproduction. For these sets, we had  $\chi^2/(\text{data point}) \simeq 1.24$  in the  $\pi N$  channel, and  $\chi^2/(\text{data point}) \simeq 2.85$  in the  $\pi\pi N$  channel.

The values of  $\chi^2/(\text{data point})$  estimated for single-pion production with 6 sets of  $N^*$  photocouplings found in Fit B were significantly larger than in Fit A:  $\chi^2/(\text{data point}) > 1.31$ . So only the sets of  $N^*$  photocouplings found in Fit A, where we restricted the variation of the  $D_{13}(1520)$ ,  $F_{15}(1680)$  photocouplings by the ranges determined from  $\pi$  electroproduction data, allow us to get

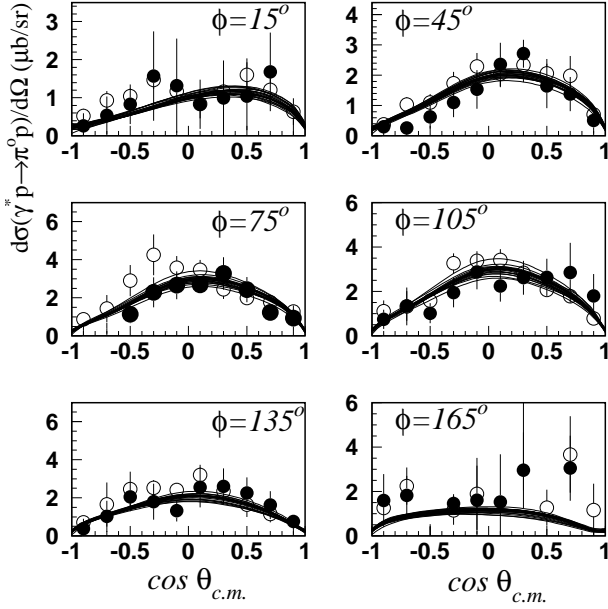


FIG. 5: Differential cross section for  $\gamma^*p \rightarrow \pi^0 p$  at  $W = 1.52 \text{ GeV}$ . The data are from CLAS [12]. Open and solid circles correspond to measurements with  $E_e = 1.645$  and  $2.445 \text{ GeV}$ , respectively. The curves correspond to the sets of the  $\gamma^*p \rightarrow N^{*+}$  helicity amplitudes obtained in the final step of our analysis (step 3).

good description of both single- and double-pion electroproduction observables.

To determine the ranges of  $\gamma^*N \rightarrow N^*$  helicity amplitudes corresponding to the best description of  $\pi$  and  $2\pi$  electroproduction data combined, we have repeated fitting both exclusive channels by applying photocoupling variations around the mean values for 3 selected sets of  $N^*$  photocouplings. Parameters  $\sigma$  in normal distributions were set at the dispersions equal to the ranges of 3 selected values of photocouplings for each resonance except  $S_{31}(1620)$ ,  $D_{13}(1700)$ ,  $D_{33}(1700)$ , and  $P_{13}(1720)$ . As the photocouplings for these states are strongly affected by the data from  $\pi\pi N$  channel (Table 2), their uncertainties in the variation procedure were taken according to the results of " $2\pi$  analysis (step 2)". W-independent multiplicative factors for the Fig. 2 exchange mechanisms in double-pion electroproduction were varied within 5% relative to the values obtained at the previous step. The non-resonant contributions for  $\pi$  electroproduction were fixed at the values used in step 1. The above described procedure for combined fit of  $\pi N$  and  $\pi\pi N$  channels was repeated. Finally, we selected 30 sets of  $N^*$  photocouplings which provide simultaneously good description of the data in both channels. Average values and dispersions for selected sets of photocouplings were attributed to the mean values and uncertainties for  $N^*$  photocouplings that were extracted in the combined analysis. They are presented in Table 2 in the columns corresponding to " $1\pi - 2\pi$  analysis".

The quality of our description of single- and double-

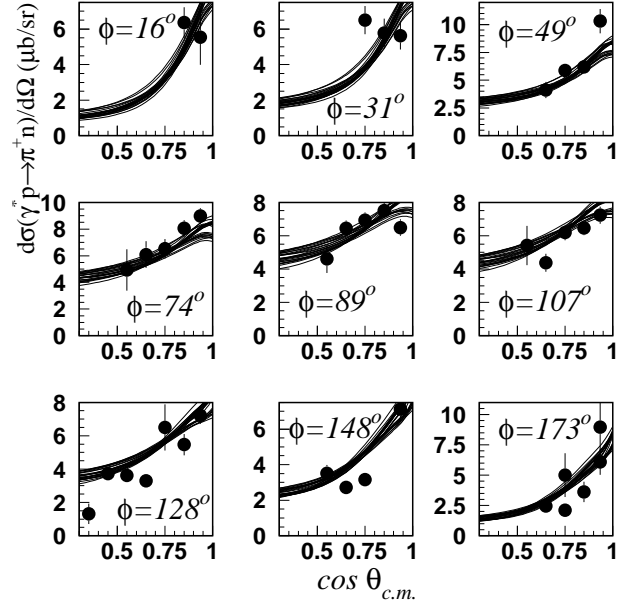


FIG. 6: Differential cross section for  $\gamma^*p \rightarrow \pi^+ n$  at  $W = 1.535 \text{ GeV}$ . The data are from DESY [18]. The curves correspond to the sets of the  $\gamma^*p \rightarrow N^{*+}$  helicity amplitudes obtained in the final step of our analysis (step 3).

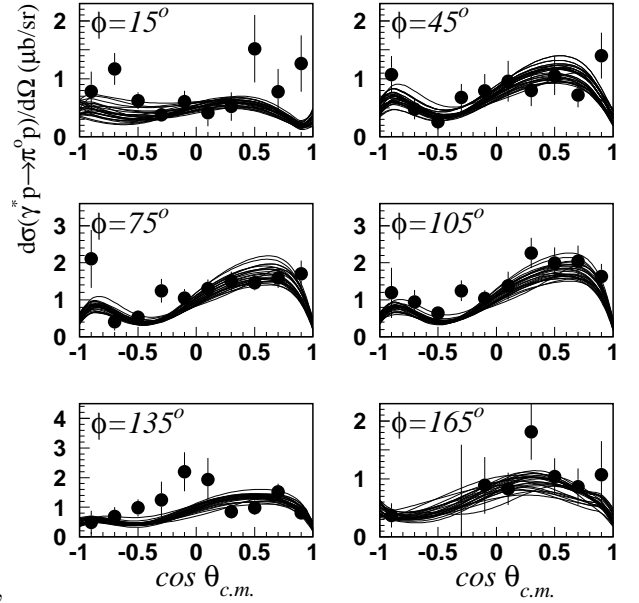


FIG. 7: The same as in Fig. 5 at  $W=1.68 \text{ GeV}$ .

pion electroproduction data is demonstrated in Figs. 5-12 where we present the results corresponding to the selected 30 sets of  $N^*$  photocouplings in comparison with experimental data. The results for the invariant mass and angular distributions are presented in the centers of the second and third resonance regions (Figs. 5-8,10,11). The data for polarized beam asymmetry in  $\pi^0$  and  $\pi^+$  electroproduction [14, 15] extend from threshold to  $W = 1.58 \text{ GeV}$ , with bins equal to  $0.04 \text{ GeV}$ . In Fig.

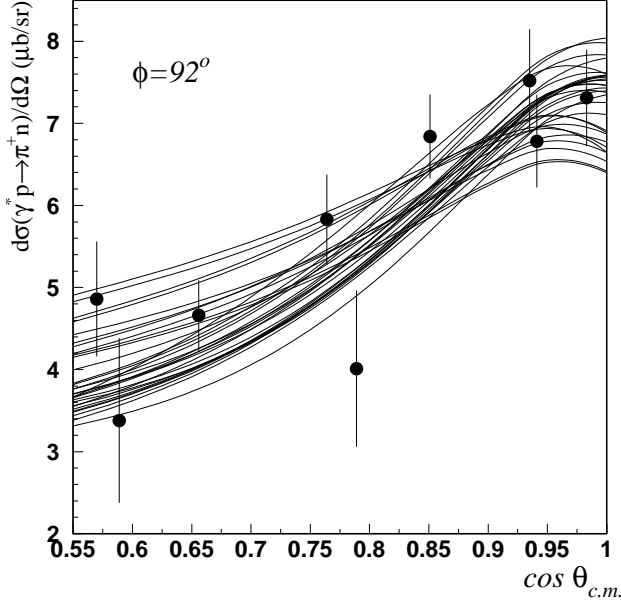


FIG. 8: Differential cross section for  $\gamma^* p \rightarrow \pi^+ n$  at  $W = 1.685$  GeV. The data are from DESY [20]. The curves correspond to the sets of the  $\gamma^* p \rightarrow N^{*+}$  helicity amplitudes obtained in the final step of our analysis (step 3).

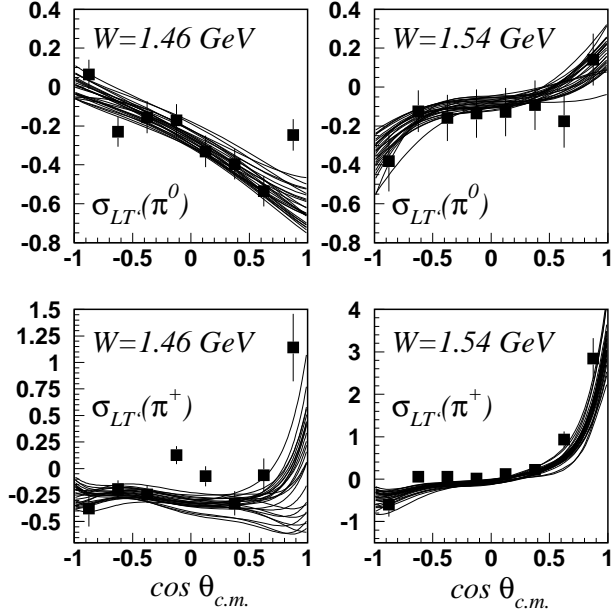


FIG. 9: Structure function  $\sigma_{LT'}$  for  $\gamma^* p \rightarrow \pi^0 p$  and  $\gamma^* p \rightarrow \pi^+ n$ . The data are from CLAS [14, 15]. The curves correspond to the sets of the  $\gamma^* p \rightarrow N^{*+}$  helicity amplitudes selected in the final step of our analysis (step 3).

9, we present the results for this observable at the energies, which are characteristic for the second resonance region; the results are presented in the form of the structure function  $\sigma_{LT'}$ . We have also presented the energy dependence of the  $2\pi$  electroproduction total cross section (Fig. 12). From Figs. 5-12 it can be seen that the

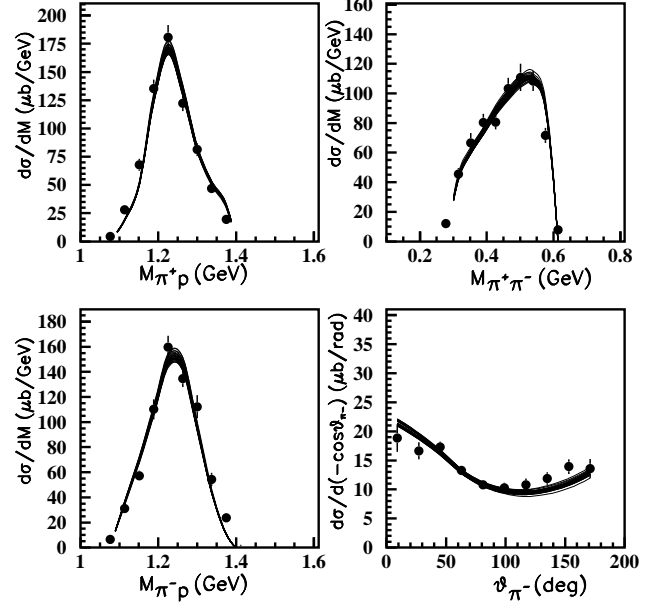


FIG. 10:  $\pi^+ p$ ,  $\pi^- p$ ,  $\pi^+ \pi^-$  invariant mass and c.m.s.  $\pi^-$  angular distributions in  $2\pi$  electroproduction at  $W = 1.54$  GeV. The data are from CLAS [10]. The curves correspond to the sets of the  $\gamma^* p \rightarrow N^{*+}$  helicity amplitudes obtained in the final step of our analysis (step 3).

calculations made with the 30 selected sets of  $N^*$  photocouplings are in good agreement with the data. The calculated curves are inside the data uncertainties, except for a few data points.

As it follows from Table 2, the results obtained in the final step of our analysis for the photocouplings of the resonances  $D_{13}(1520)$ ,  $S_{11}(1650)$ , and  $F_{15}(1685)$  coincide within errors with those obtained separately in the analyses of single- and double-pion electroproduction data. The errors of these photocouplings obtained in combined analysis are considerably lower than those found in "2 $\pi$  analysis", while comparable with "1 $\pi$  analysis" errors. Therefore, single-pion electroproduction data considerably affect the results on photocouplings for low-lying states with masses below 1.7 GeV and sizable decay rates to the  $\pi N$  final state. As for the  $pA_{1/2}$   $P_{11}(1440)$  amplitude,  $\pi$  electroproduction data have small sensitivity to its change from the value obtained in the step 1 to one found in the final step. As it follows from the results of the final step of our analysis, the small error bar for this amplitude, derived in step 1, is related just to the way of evaluation of uncertainties in  $\pi$  electroproduction data fit, when only global minimum of  $\chi^2$  was taken into account.

For the resonances with major decay rates to the  $2\pi N$  channel ( $S_{31}(1620)$ ,  $D_{13}(1700)$ ,  $D_{33}(1700)$ ,  $P_{13}(1720)$ ), the photocouplings obtained in combined analysis coincide within the errors with the results of "2 $\pi$  analysis".



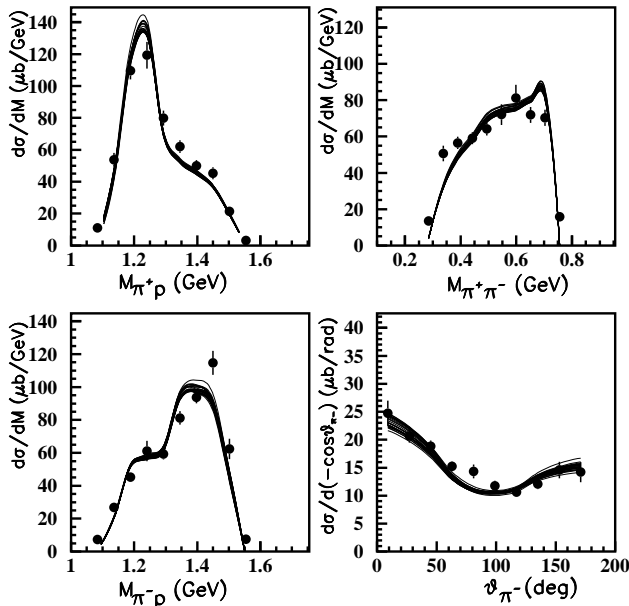


FIG. 11: The same as in Fig. 10 at  $W=1.69$  GeV.

However, the combined analysis allowed us to considerably reduce the uncertainties of these photocouplings compared with those derived in the analysis of two-pion electroproduction data only. The results of the combined analysis for  $S_{31}(1620)$ ,  $D_{13}(1700)$ ,  $D_{33}(1700)$ , and  $P_{13}(1720)$  are mostly different from those of "1 $\pi$  analysis". Nevertheless, as it can be seen from Figs. 5-9, the photocouplings for these states obtained in combined analysis allow us to describe single-pion electroproduction data.

In Table 3, we compare our results for the transverse photocouplings of the resonances from the  $[70, 1^-]$  multiplet with the predictions of single quark transition model (SQTm) [32]. This approach is based on the assumptions that  $SU(6) \otimes O(3)$  symmetry holds for the leading part of confinement forces and only a single quark is affected in the electroexcitation of the  $N^*$ . For the states assigned to the same  $SU(6) \otimes O(3)$  multiplet, this approximation allows us to relate transverse  $N^*$  photocouplings to limited number of parameters, which are three in the case of the  $[70, 1^-]$  multiplet. In Ref. [32], these parameters were found from the experimental data on the  $S_{11}(1535)$  and  $D_{13}(1520)$  photocouplings, and the predictions were made for the transverse photocouplings of all other states assigned to  $[70, 1^-]$ .

As it can be seen, the photocouplings for all states from  $[70, 1^-]$  obtained in our analysis, except  $D_{13}(1700)$ , are in good agreement with SQTm predictions. SQTm results for  $D_{13}(1700)$  were obtained using mixing angle  $\simeq 6^\circ$  between  $|N^2, \frac{3}{2}^- \rangle$  and  $|N^4, \frac{3}{2}^- \rangle$  configurations found in the analysis of  $D_{13}(1700)$  hadronic decays [27]. Accuracy of these data still remains poor. One can get reasonable

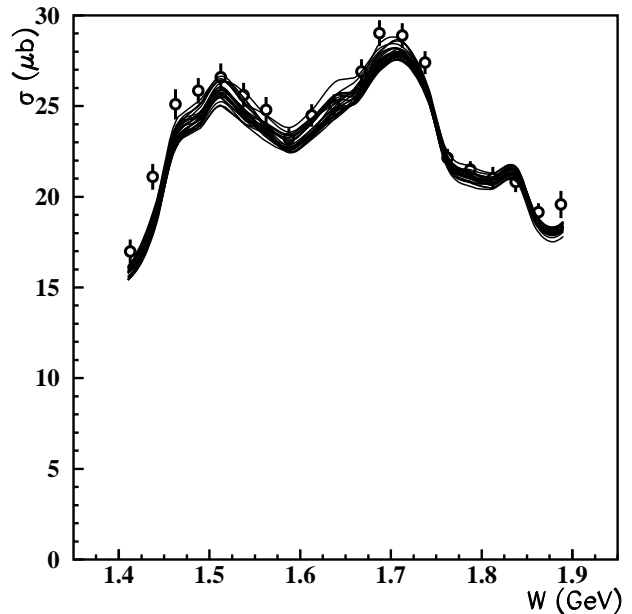


FIG. 12: Total cross section for  $2\pi$  electroproduction. The curves corresponds to the sets of the  $\gamma^*p \rightarrow N^{*+}$  helicity amplitudes obtained in the final step of our analysis (step 3).

SQTm reproduction of our results for  $D_{13}(1700)$ , if instead of  $6^\circ$ , a mixing angle  $\simeq 20^\circ$  is used. Good overall agreement of our results for the  $N^*$  photocouplings with SQTm predictions strongly supports the complicated dynamics of  $N^*$  formation and electroexcitation is determined mostly by the  $SU(6) \otimes O(3)$  spin-flavor-space symmetry, and only a single quark is affected in the electroexcitation of the  $N^*$ .

#### IV. CONCLUSION

Recent CLAS and world data on single- and double-charged pion electroproduction off protons are successfully described in the second and third resonance regions using common values of  $N^*$  photocouplings. The analysis was carried out using isobar models of Refs. [8, 21] and [24, 25, 26] for single- and double-pion electroproduction, respectively. The non-resonant mechanisms in these exclusive channels are completely different. Therefore, a successful description of  $\pi N$  and  $\pi\pi N$  channels combined strongly suggests that: a) we achieved reasonable treatment of non-resonant mechanisms; b) a phenomenological separation between  $N^*$  and background contributions made according to isobar models [8, 21] and [24, 25, 26] is reliable in both channels; and (c) extracted  $N^*$  photocouplings, which provide good description of all measured observables in these channels, have considerably reduced model uncertainties.

From our combined analysis, the  $\gamma^*p \rightarrow N^{*+}$  helicity

$N^*$	$M$	$\tilde{M}$	$\Gamma$	$\tilde{\Gamma}$	$\beta_{\pi N}$	$\tilde{\beta}_{\pi N}$	$\beta_{\pi\Delta+\rho N}$	$\tilde{\beta}_{\pi\Delta+\rho N}$
	(MeV)	(MeV)	(MeV)	(MeV)	(%)	(%)	(%)	(%)
$P_{11}(1440)$	1430 – 1470	1440	250 – 450	350	60 – 70	60	20 – 30	25
$D_{13}(1520)$	1515 – 1530	1520	110 – 135	120	50 – 60	50	30 – 50	33
$S_{31}(1620)$	1615 – 1675	1620	120 – 180	150	20 – 30	25	70 – 80	75
$S_{11}(1650)$	1640 – 1680	1650	145 – 190	150	55 – 90	70	5 – 19	5
$F_{15}(1680)$	1675 – 1690	1680	120 – 140	130	60 – 70	65	8 – 30	17
$D_{33}(1700)$	1670 – 1770	1700	200 – 400	300	10 – 20	15	80 – 90	85
$D_{13}(1700)$	1650 – 1750	1700	50 – 150	100	5 – 15	10	85 – 95	90
$P_{13}(1720)$	1650 – 1750	1720	100 – 200	150	10 – 20	15	> 70	85

TABLE I: List of masses, widths and branching ratios of the investigated resonances. The quoted ranges are taken from RPP [29]. The quantities labeled by tildes correspond to the values used in our analysis.

amplitudes are extracted for the resonances  $P_{11}(1440)$ ,  $D_{13}(1520)$ ,  $S_{31}(1620)$ ,  $S_{11}(1650)$ ,  $F_{15}(1680)$ ,  $D_{33}(1700)$ ,  $D_{13}(1700)$ , and  $P_{13}(1720)$ .

Our results for the transverse photocouplings of the resonances from the  $[70, 1^-]$   $SU(6) \otimes O(3)$  multiplet are

in good agreement with the predictions of the single quark transition model [32]. Thus, we have strong evidence for  $SU(6)$  as a leading symmetry of confinement forces and single-quark transitions as dominant mechanism in  $N^*$  excitation by photons.

- 
- [1] V. D. Burkert, T.-S.H. Lee, Int. J. Mod. Phys. **E13**, 1035 (2004).
  - [2] B. Krusche et al., Phys. Lett. **B358**, 40 (1995).
  - [3] R. Thompson et al., CLAS Collaboration, Phys. Rev. Lett. **86**, 1702 (2001).
  - [4] O. Bartalini et al., Phys. Lett. **B544**, 113 (2002).
  - [5] Wen-Tai Chiang, Shin Nan Yang, L. Tiator, and D. Drechsel, Nucl. Phys. **A700**, 429 (2002).
  - [6] M. Dugger et al., Phys. Rev. Lett. **89**, 222002 (2002).
  - [7] I. G. Aznauryan, Phys. Rev. **C68**, 065204 (2003).
  - [8] I. G. Aznauryan, V. D. Burkert, H. Egiyan, et al., Phys. Rev. **C71**, 015201 (2005).
  - [9] V. Crede et al., Phys. Rev. Lett. **94**, 012004 (2005).
  - [10] M. Ripani et al., Phys. Rev. Lett. **91**, 022002 (2003).
  - [11] CLAS Physics Data Base, <http://clasdb3.jlab.org>.
  - [12] K. Joo et al., CLAS Collaboration, Phys. Rev. Lett. **88**, 122001 (2002).
  - [13] H. K. Egiyan et al., CLAS Collaboration, to be submitted to Phys. Rev. C; L. C. Smith (for CLAS Collaboration), hep-ph/0306199.
  - [14] K. Joo et al., CLAS Collaboration, Phys. Rev. **C68**, 032201 (2003).
  - [15] K. Joo et al., CLAS Collaboration, Phys. Rev. **C70**, 042201 (2004).
  - [16] Ch. Gerhardt et al., Preprint DESY-F21-71/3 (1971)
  - [17] W. J. Shuttleworth et al., Nucl. Phys. **B45**, 428 (1972).
  - [18] J. C. Alder et al., Nucl. Phys. **B99**, 1 (1975).
  - [19] J. C. Alder et al., Nucl. Phys. **B105**, 253 (1976).
  - [20] Ch. Gerhardt et al., Preprint DESY-F21-79/02 (1979)
  - [21] I. G. Aznauryan, Phys. Rev. **C67**, 015209 (2003).
  - [22] R. A. Arndt, I. I. Strakovski, and R. L. Workman, Phys. Rev. **C53**, 430 (1996).
  - [23] R. A. Arndt, W. J. Briscoe, I. I. Strakovski, and R. L. Workman, Phys. Rev. **C66**, 055213 (2002).

$N^*$	1 $\pi$ analysis (step 1)			2 $\pi$ analysis (step 2)			1 $\pi - 2\pi$ analysis (step 3)		
	$pA_{1/2}$	$pA_{3/2}$	$pS_{1/2}$	$pA_{1/2}$	$pA_{3/2}$	$pS_{1/2}$	$pA_{1/2}$	$pA_{3/2}$	$pS_{1/2}$
$P_{11}(1440)$	$4 \pm 4$ ( $23 \pm 4$ )		$40 \pm 4$	$21 \pm 9$		$35 \pm 6$	$21 \pm 4$		$33 \pm 6$
$D_{13}(1520)$	$-67 \pm 3$	$62 \pm 4$	$-38 \pm 3$	$-62 \pm 12$	$62 \pm 11$	$-40 \pm 7$	$-65 \pm 4$	$62 \pm 5$	$-35 \pm 3$
$S_{31}(1620)$	$31 \pm 3$		$-35 \pm 3$	$13 \pm 3$		$-25 \pm 4$	$16 \pm 4$		$-28 \pm 3$
$S_{11}(1650)$	$43 \pm 2$		$-12 \pm 2$	$44 \pm 16$		$-8 \pm 2$	$43 \pm 7$		$-6 \pm 3$
$F_{15}(1680)$	$-38 \pm 4$	$56 \pm 2$	$-18 \pm 2$	$-31 \pm 8$	$52 \pm 10$	$-14 \pm 3$	$-32 \pm 5$	$51 \pm 4$	$-15 \pm 3$
$D_{33}(1700)$	$58 \pm 5$	$29 \pm 3$	$-15 \pm 5$	$49 \pm 8$	$36 \pm 8$	$-11 \pm 4$	$44 \pm 4$	$36 \pm 4$	$-7 \pm 4$
$D_{13}(1700)$	$-6 \pm 8$	$-55 \pm 7$	$0 \pm 8$	$-19 \pm 3$	$11 \pm 2$	0	$-21 \pm 2$	$10 \pm 1$	0
$P_{13}(1720)$	$45 \pm 6$	$-48 \pm 7$	$0 \pm 7$	$56 \pm 6$	$-62 \pm 9$	0	$55 \pm 3$	$-68 \pm 4$	0

TABLE II: Helicity amplitudes for the  $\gamma^*p \rightarrow N^{*+}$  transitions (in  $10^{-3}GeV^{-1/2}$  units) obtained at different steps of our analysis. Final results are presented in the columns corresponding to "1 $\pi - 2\pi$  analysis". In the brackets, we present the  $pA_{1/2}$   $P_{11}(1440)$  amplitude found in the dispersion relations analysis of pion electroproduction in Ref. [8]; this is the only result of this analysis which is different from that found using isobar model.

Resonance	Our results		SQTM	
	$pA_{1/2}$	$pA_{3/2}$	$pA_{1/2}$	$pA_{3/2}$
$D_{13}(1520)$	$-65 \pm 4$	$62 \pm 5$	$-78 \pm 10$	$63 \pm 3$
$S_{31}(1620)$	$16 \pm 4$		$18 \pm 3$	
$S_{11}(1650)$	$43 \pm 7$		$43 \pm 3$	
$D_{33}(1700)$	$44 \pm 4$	$36 \pm 4$	$50 \pm 5$	$35 \pm 5$
$D_{13}(1700)$	$-21 \pm 2$	$10 \pm 1$	$-7 \pm 2$	$6 \pm 2$

TABLE III: Our results for the resonances of the  $[70, 1^-]$  multiplet (in  $10^{-3}GeV^{-1/2}$  units) in comparison with the predictions of single quark transition model [32].

- [24] V. Mokeev et. al., Proceedings of NSTAR2004 workshop , March 24-27, 2004, Grenoble, France, World Scientific, ed. by J.-P. Bocquet, V. Kuznetsov, D. Rebreyend, 317.
- [25] M. Ripani et. al., Nucl. Phys, **A672**, 220 (2000).
- [26] V. Mokeev et. al., Phys. of Atom. Nucl. **64**, 1292 (2001).
- [27] T. P. Vrana et. al., Phys. Rep., **328**, 181 (2000).
- [28] M.Bellis, et.al. (CLAS Collaboration), Proceedings of NSTAR2004 workshop , March 24-27, 2004, Grenoble, France, World Scientific, ed. by J.-P. Bocquet, V. Kuznetsov, D. Rebreyend, 139.
- [29] Review of Particle Physics, S. Eidelman et al., Phys. Lett. **B592**, 1 (2004).
- [30] F.James. MINUIT Minimization package reference manual. CERN Program Library Long Writeup D506.

- [31] V.D. Burkert, et. al., Proc. of the 17 International UPAP Conference on Few-Body Problems in Physics, Durham. NC, USA, 5-10 June 2003, Elsevier, 2004, ed.by W. G. Glöckle, W. Tornow, S231.
- [32] V.D. Burkert, et. al., Phys. Rev. **C67**, 035204 (2003).